

Modeling the Impact of a Falling Rock Cluster on Rigid Structures

Ge Gao¹ and Mohamed A. Meguid, P.Eng., M.ASCE²

Abstract: Rockfall is a common geological hazard in mountainous areas and can pose great danger to people and properties. Understanding the impact forces induced by a single rock or a rock cluster on retaining structures is considered key in the analysis and design of protection barriers. This study presents the results of small-scale laboratory experiments conducted to measure the impact forces induced by a group of rocks moving down a rough slope on a barrier wall. The effect of slope inclination angle and wall location on the impact pressure acting on the wall was examined. A three-dimensional discrete element model was then proposed and used to study the behavior of the rock cluster under different geometric conditions. Rocks were modeled using polydisperse clumps in which each clump consisted of several overlapping spherical particles to account for the shape effect of the falling rocks. First, the model was validated by comparing the measured and calculated forces, and then, it was used to investigate the role of different material and geometric parameters on the impact behavior. Conclusions were made regarding the role of modeling the irregular rock shapes and the roughness of the slope surface on the behavior impacted by the travel mode for different slope angles. DOI: [10.1061/\(ASCE\)GM.1943-5622.0001045](https://doi.org/10.1061/(ASCE)GM.1943-5622.0001045). © 2017 American Society of Civil Engineers.

Author keywords: Rockfall analysis; Discrete element; Impact force measurement; Protective barriers.

Introduction

Gravity-driven rockfall is generally characterized by extreme rapidity and long traveled distance. Rockfall usually involves a sudden movement of either a single rock or a group of rocks that detach from the rock face and can lead to property damage, personal injury, and even loss of life when people, vehicles, or railways are in the rock-movement path. Mitigation measures are, therefore, critical at vulnerable locations and may include the installation of engineered protection structures, such as flexible rock fences, catchment ditches, or rigid barriers. Catchment areas are often used along transportation corridors to retain a large volume of rock. However, a significantly large catchment area may be needed for high slopes, but is sometimes limited by the right-of-way acquisition. Wall-type structures require a small footprint and can be constructed using stiff material (concrete or timber) or flexible material (rock fences). Because they are prone to damage by high-energy events, rigid walls are used for relatively low-energy impacts (Turner and Schuster 2013).

Understanding the mechanics of rockfall and the possible impact force on rigid barriers under various conditions is important to the design of protection systems.

Previous studies [e.g., Basson (2012); Wei et al. (2014)] and field observations [e.g., Giani et al. (2004); Alejano et al.

(2007); Spadari et al. (2012)] showed that falling rocks experience different types of motion along the path, including free falling, rolling, bouncing, and sliding. Ritchie (1963) investigated the movement pattern of rockfall and produced design criteria to determine the geometry of the catchment area according to slope height and inclination angle. Rockfall analysis was generally performed to assess the rockfall velocity and impact energy using either empirical approaches or numerical simulations (Turner and Schuster 2013).

Different computational modeling approaches are available to simulate rockfall, including lumped mass, rigid-body dynamics, and discrete-element analysis. The lumped-mass approach assumes that a falling rock can be represented by a single material point that has a concentrated mass, ignoring the effect of the rock shape, size, and rotation (Guzzetti et al. 2002; Agliardi and Crosta 2003). The rigid-body model, developed by Descouedres and Zimmermann (1987), is a three-dimensional (3D) kinetic-impact model used to simulate rolling, impact, and rebound motions (Frattini et al. 2008; Agliardi et al. 2009). The method uses kinematics and equations of motion to analyze a collision by assuming instantaneous contact on small contact areas between colliding bodies. The discrete-element method (DEM), introduced by Cundall and Strack (1979), has attracted great attention over the last few decades to model rockfall hazard [e.g., Magnier and Donzé (1998); Nicot et al. (2001); Plassiard and Donzé (2009); Wang and Tonon (2011); Chen et al. (2013); Bonilla-Sierra et al. (2015)]. Various discrete-element approaches are available to reproduce the irregular shape and geometry of moving rock. The impact forces between two entities are generally obtained using different contact models and explicit time-stepping algorithms. Compared with other methods of rockfall analysis (lumped mass and rigid-body dynamics), the DEM is considered to be more rigorous and can accurately replicate trajectories and rolling and sliding behaviors. It also models crack propagation and breakage of the falling body.

A considerable number of experimental and numerical studies have been reported in the literature that evaluated rockfall impact

¹Graduate Student, Dept. of Civil Engineering and Applied Mechanics, McGill Univ., 817 Sherbrooke St. W., Montreal, QC, Canada H3A 0C3. E-mail: ge.gao2@mail.mcgill.ca

²Associate Professor, Dept. of Civil Engineering and Applied Mechanics, McGill Univ., 817 Sherbrooke St. W., Montreal, QC, Canada H2A 0C3 (corresponding author). ORCID: <https://orcid.org/0000-0002-5559-194X>. E-mail: mohamed.meguid@mcgill.ca

Note. This manuscript was submitted on September 12, 2016; approved on July 31, 2017; published online on November 28, 2017. Discussion period open until April 28, 2018; separate discussions must be submitted for individual papers. This paper is part of the *International Journal of Geomechanics*, © ASCE, ISSN 1532-3641.

on various protection systems, including drapery [e.g., Thoeni et al. (2014)], embankments [e.g., Plassiard and Donzé (2009)], and rigid walls [e.g., Kishi et al. (2000)]. Although these studies provide some comprehension of the impact mechanics of rockfall on barrier systems, quantification through measurements of impact forces induced by a rock cluster on vertical walls is needed.

Scope and Objective

The objective of this study was to investigate the impact forces exerted by a group of rocks moving down a rough slope using 3D discrete-element analysis. Using tactile sensing technology, laboratory experiments were first conducted to measure the impact forces induced by two different rock clusters on an instrumented wall. The experimental results were used to validate the discrete element model that had been developed and used throughout this study. Emphasis was placed on modeling the irregular-shaped geometry of the rocks and the slope roughness and inclination angles. The results presented in this paper provide new insights into understanding the impact mechanics of a falling rock cluster on rigid structures.

Experimental Study

A flume measuring 1.82 m in length, 0.6 m in width, and 0.3 m in depth was constructed and used in this study to simulate rockfall on a rough surface. The flume was supported by a steel structure that allows the slope angle to be adjusted. Three inclination angles (α) were examined in this study: 30, 45, and 60° (Fig. 1). The sidewalls and the release box were made of transparent plexiglass material such that the rock movement was monitored using a video camera. An instrumented wall was placed at different locations from the toe of the slope and used to measure the impact pressure induced by two different rock clusters.

To create a realistic slope surface, the flume was lined with a 1.5-mm ebonite sheet perforated with 202 circular openings, each with diameter of 5.0 cm, staggered at 8.0-cm center spacing. This bumpy surface allowed for the dynamic nature of the rockfall, including sliding, bouncing, and rolling, to be captured. Local river stones obtained from the Montreal area were selected for this experimental work. The stones (Fig. 2) were nearly rounded with diameters that ranged between 3.0 and 9.0 cm. This rock material was found to provide sufficient impact force that could be measured with reasonable accuracy. The experiments were repeated for two rock clusters: C_1 , consisted of 53 stones (total mass = 8.0 kg), and C_2 , had 99 stones (total mass = 13.0 kg). The properties of the used material are listed in Table 1.

Instrumented Wall

A rigid vertical wall 0.6 and 0.3 m in width and height, respectively, was connected to the horizontal run-out base using a steel frame as illustrated in Fig. 3. The wall location was adjustable such that four different separation distances (x) from the toe of the slope were investigated: 0.0, 0.25, 0.4, and 0.6 m. Both the wall side facing the slope and the preceding landing areas were instrumented using TactArray pressure sensors (PPS, Los Angeles) with capacities of 345 and 138 kPa for the wall and the landing area, respectively (Fig. 3). Sensing pads generally consist of two sets of orthogonal electrode plates separated by a dielectric matrix that acts as a spring allowing for the flexibility of the pad design. Each pad consisted of 256 square sensing cells arranged continuously and controlled using a data acquisition system (Ahmed et al. 2015). In addition to the manufacturer's

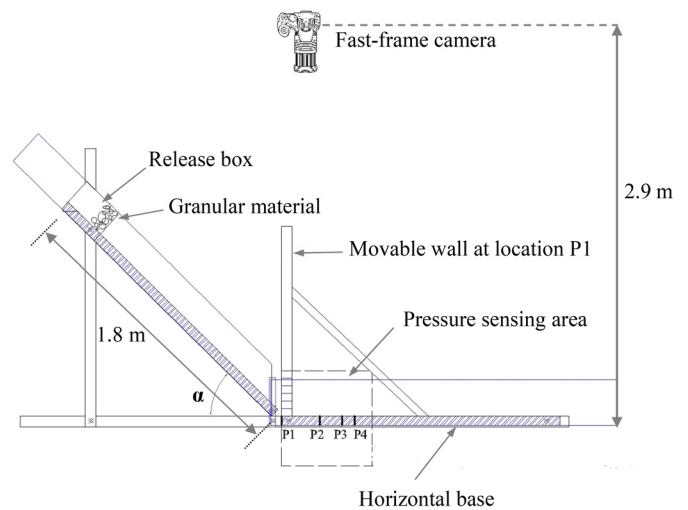


Fig. 1. Schematic of the test setup for α measures of 30, 45, and 60°



(a)



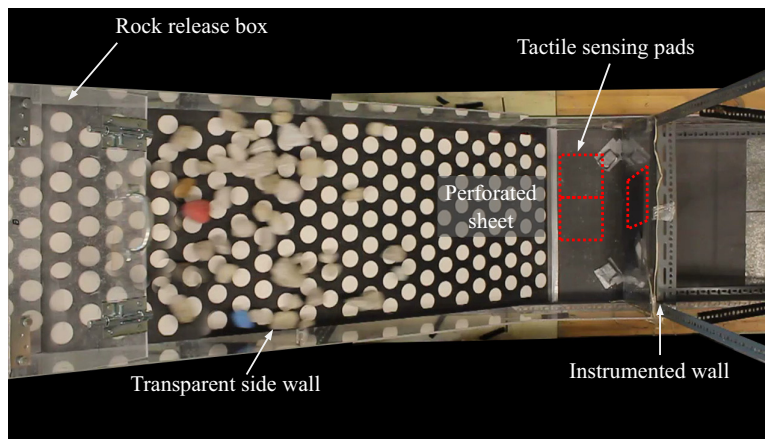
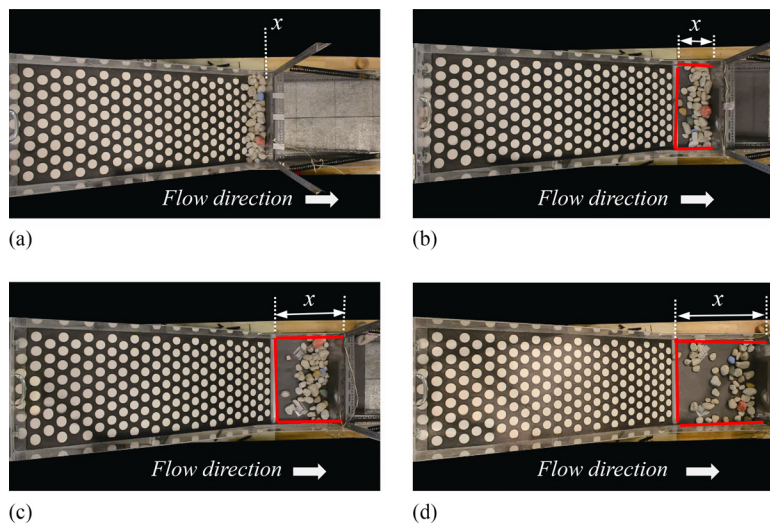
(b)

Fig. 2. Two rock clusters used in the experiments (in centimeters): (a) C_1 ; (b) C_2

calibration, the sensing pads were also calibrated with river stones of known weight, and the total force was recorded using the data acquisition system.

Table 1. Material Properties of the Two Rock Clusters Used in the Experiments

Cluster (kg)	Density (kg/m^3)	Number of stones	Average diameter (cm)	Coefficient of uniformity	Coefficient of curvature	Volume (m^3)
C_1 (8)	2,600	53	5.1	1.6	1.0	0.006
C_2 (13)	2,600	99	5.3	1.5	0.9	0.01

**Fig. 3.** Upper view of the flume showing the instrumented wall structure**Fig. 4.** Test procedure showing the studied wall locations from the slope (in centimeters): (a) $x = 0$; (b) $x = 25$; (c) $x = 40$; (d) $x = 60$

Test Procedure and Measured Results

The stones were loosely held in the release box, which was equipped with a side-hinged door with a latch that could be opened instantaneously to initiate rockfall. The stones were released through the hinged door and allowed to travel freely down the flume toward the wall. In subsequent tests, the wall was incrementally moved away from the toe of the slope allowing for the pressure on both the vertical and horizontal sensing pads to be recorded as shown in Fig. 4.

A total of 72 experiments were conducted for the two investigated rock clusters. The tests were repeated three times for each inclination angle and separation distance. A summary of the measured impact forces for the two rock clusters, C_1 and C_2 , is provided in Table 2. The results reveal that the lateral impact force on the wall with offset distance, x , of 0 cm was rapidly increased with the

increase in slope inclination angle. In addition, as the wall offset distance from the toe increased, the impact force drastically decreased despite an increase in the slope inclination angle. For example, the impact force induced by cluster C_2 changed from 976 N for an inclined angle, α , of 60° to only 76 N when the wall moved 25 cm (or 5 times the average rock diameter). Moving the wall further away from the toe of the slope to a distance of 60 cm resulted in the impact force decreasing to 3 N. The measured forces for α values of 30 and 45° were found to be 17 and 7 N, respectively, for rock cluster C_2 , which were greater than that for the case in which x was 60 cm and significantly greater than the results for an α measure of 60° . This behavior may be attributed to the travel mode experienced by the falling rock cluster for an α of 60° , which was dominated by rapid sliding with a limited impact area near the toe. Vertical pressures were also measured on the landing surface near

the wall for various offset distances and are presented in Table 3. These pressure values were found to be much smaller at this location than the lateral pressure values on the wall.

Numerical Analysis

A 3D discrete-element model was built with the commercial software package *PFC3D* using a soft-contact approach for which deformations occur at the contacts between the rigid bodies (e.g., balls, clumps, and walls). The contact mechanics among these bodies are briefly described in this section.

The overlap ΔU^n of Particle A in contact with Particle B and a wall is defined as

$$\Delta U^n = \begin{cases} R_A + R_B - d, & \text{Ball-ball} \\ R_A - d, & \text{Ball-wall} \end{cases} \quad (1)$$

where R = particle radius; and d = distance between the centers of the two particles or the shortest distance between the center of the particle and the wall.

The contact force vector, F_C , which represents the interaction of Particles A and B for all-ball contact or the action of the ball on the

Table 2. Measured Impact Force on the Wall for Different Offset Distances and Slope Inclination Angles

Distance [x (cm)]	Test	Impact force (N)					
		Cluster C ₁ (8 kg)			Cluster C ₂ (13 kg)		
		Inclination angle (degrees)			Inclination angle (degrees)		
		30	45	60	30	45	60
0	1	80.1	190.4	1,000.5	280.2	650.3	950.2
	2	91.7	259.9	852.9	250.9	609.4	996.5
	3	84.5	283.0	872.7	243.7	690.1	981.6
	Average	85.4	244.4	908.7	258.3	649.9	976.1
	Standard deviation	5.8	48.2	80.1	19.4	40.4	23.7
25	1	30.7	42.2	15.2	49.9	65.2	85.3
	2	20.4	29.6	2.7	33.7	50.3	70.1
	3	16.2	28.7	9.0	35.3	52.8	72.4
	Average	22.4	33.5	9.0	39.6	56.1	76.0
	Standard deviation	7.5	7.5	6.3	8.9	8.0	8.2
40	1	22.6	18.4	4.3	43.6	40.2	28.1
	2	16.8	11.0	1.2	27.6	38.7	20.1
	3	14.0	19.4	2.4	25.7	28.2	29.1
	Average	17.8	16.3	2.6	32.3	35.7	25.8
	Standard deviation	4.4	4.6	1.5	9.8	6.5	4.9
60	1	5.2	6.2	0.6	14.2	10.2	5.6
	2	1.7	9.0	1.4	27.6	8.4	2.1
	3	4.1	3.0	2.8	7.7	2.8	2.6
	Average	3.7	6.1	1.6	16.5	7.1	3.4
	Standard deviation	1.8	3.0	1.1	10.1	3.9	1.9

Table 3. Measured Impact Force on the Landing Surface for Different Offset Distances and Slope Inclination Angles

Distance [x (cm)]	Test	Impact force (N)					
		Cluster C ₁ (8 kg)			Cluster C ₂ (13 kg)		
		Inclination angle (degrees)			Inclination angle (degrees)		
		30	45	60	30	45	60
25	1	46.0	83.1	82.0	60.9	165.5	128.5
	2	40.3	64.8	81.1	57.7	129.3	138.2
	3	39.4	74.0	75.1	48.2	172.4	119.6
	Average	41.9	74.0	79.4	55.6	155.8	128.8
	Standard deviation	3.6	9.1	3.8	6.6	23.1	9.3
40	1	28.6	22.4	61.7	30.6	65.2	105.1
	2	26.8	19.3	49.2	28.6	58.3	97.3
	3	34.2	24.2	55.0	27.4	60.5	90.3
	Average	29.9	21.9	55.3	28.9	61.3	97.6
	Standard deviation	3.9	2.5	6.3	1.6	3.5	7.4
60	1	15.8	15.3	37.5	21.4	29.2	68.4
	2	25.2	11.3	39.7	20.7	32.6	75.2
	3	20.3	13.4	33.5	25.8	31.0	59.3
	Average	20.4	13.4	36.9	22.6	30.9	67.7
	Standard deviation	4.7	2.0	3.1	2.7	1.7	8.0

wall for ball–wall contact, can be resolved into normal and shear forces.

$$F_C = F_C^N + F_C^S \quad (2)$$

where F_C^N and F_C^S = normal and shear component of the contact force, respectively.

The normal and shear components of the contact force are calculated by

$$F_C^N = K^n \Delta U^n \quad (3)$$

$$\Delta F_C^S = -k^S \Delta U^S \quad (4)$$

where ΔF_C^S = incremental elastic shear force; ΔU^n = overlapping of the two particles; K^n = normal stiffness; and k^S = shear stiffness as determined using a tangent modulus. The normal and shear stiffnesses are given by

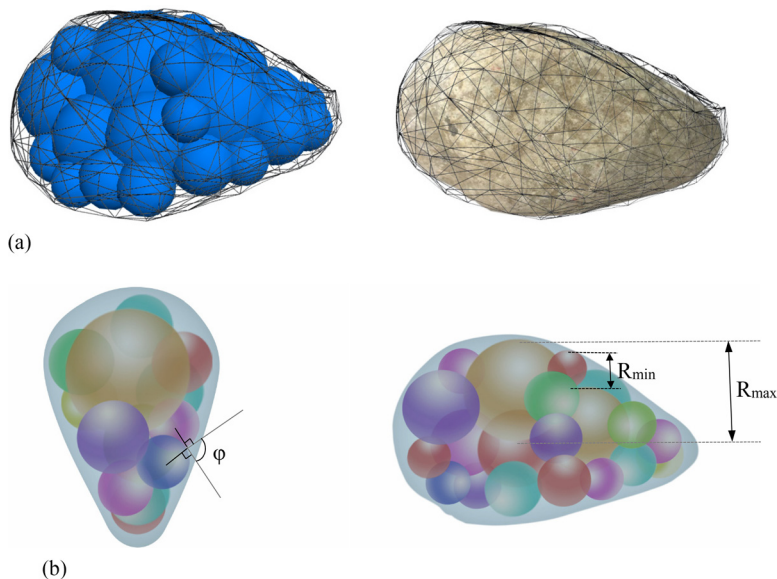


Fig. 5. Clump template used in the analysis: (a) triangulated surface that matches the 3D geometry of a rock; (b) clump representing a rock with 23 rigid spheres

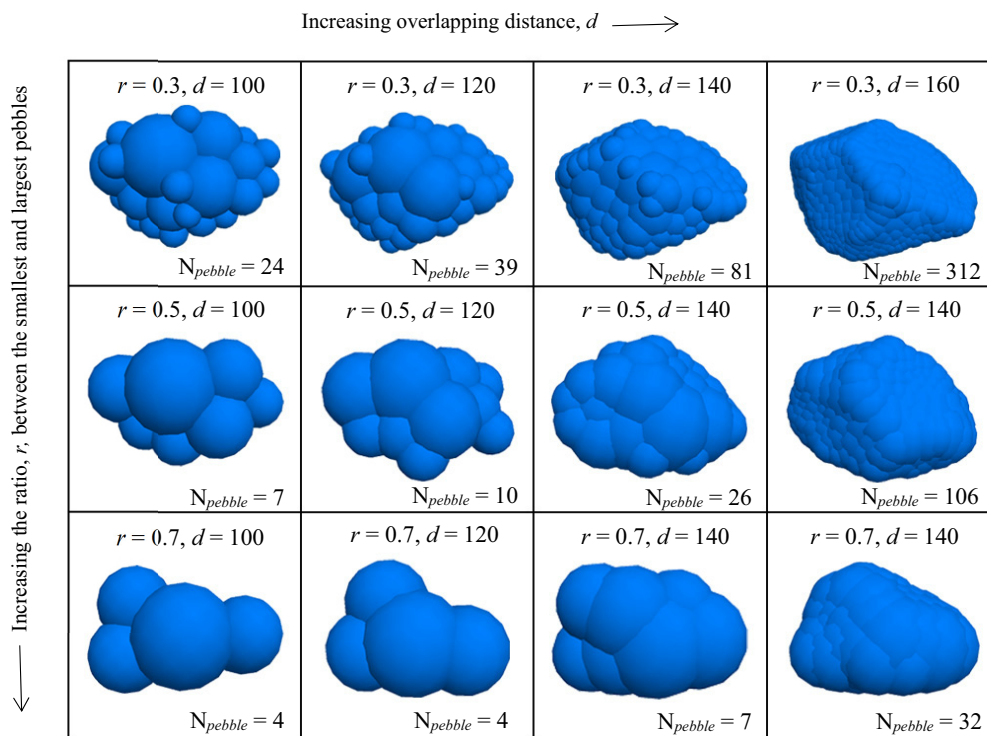
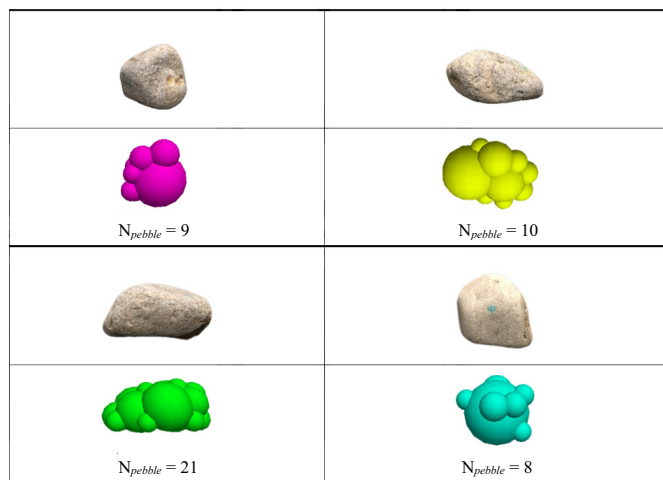
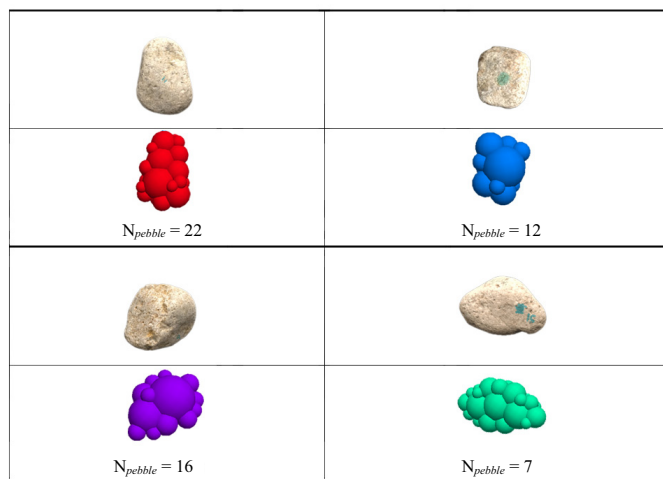


Fig. 6. Template parameters used to generate clumps that represent the rock shape



(a)



(b)

Fig. 7. Particle shapes used to build the clumps used in *PFC3D* analysis: (a) C_1 ; (b) C_2

$$K^n = \frac{k_n^A k_n^B}{k_n^A + k_n^B} \quad (5)$$

$$k^s = \frac{k_s^A k_s^B}{k_s^A + k_s^B} \quad (6)$$

A resultant force that represents all contacts on a single solid body was obtained using contact mechanics, and Newton's second law was then applied to compute accelerations. The displacement of each element was then obtained using a central difference explicit time integration described with the two following equations:

$$F_i = m(\ddot{x}_i - \mathbf{g}_i) \quad (7)$$

where F_i = sum of all externally applied forces acting on the particle; m = total mass of the body; \ddot{x}_i = particle acceleration; and \mathbf{g}_i = body force acceleration vector.

$$M_i = \dot{H}_i \quad (8)$$

where M_i = moment acting on the particle; and \dot{H}_i = particle angular momentum.

Table 4. Summary of the Measured Rebound Height and the Corresponding COR

Test	Rebound height (m)	COR
1	0.084	0.29
2	0.078	0.28
3	0.090	0.30
4	0.078	0.28
5	0.102	0.32
6	0.109	0.33
7	0.073	0.27
8	0.096	0.31
9	0.090	0.30
10	0.102	0.32
11	0.090	0.30
12	0.090	0.30
13	0.096	0.31
14	0.102	0.32
15	0.102	0.32
16	0.084	0.29
17	0.096	0.31
18	0.090	0.30
19	0.078	0.28
20	0.084	0.29
21	0.090	0.30
22	0.096	0.31
23	0.096	0.31
24	0.109	0.33
25	0.096	0.31
26	0.102	0.32
27	0.090	0.30
28	0.090	0.30
29	0.096	0.31
30	0.090	0.30

Note: Average rebound height = 0.092 m; standard deviation of rebound height = 0.009; average COR = 0.30; standard deviation of COR = 0.01.

Modeling Irregularly Shaped Rock Using Clump Templates

Rock shape is known to play a significant role in rockfall modeling, particularly when discrete-element analysis is used (Taghavi 2011). Using spherical entities to simulate irregularly shaped rock has been found to provide excessive rolling (Oda and Iwashita 1999). Researchers [e.g., Lu and McDowell (2010); Stahl and Konietzky (2011); Li et al. (2012); Indraratna et al. (2014)] applied clump logic in modeling complex-shaped particles in the DEM. A clump is a single rigid body of overlapping spherical pebbles of different sizes that acts as a single particle of a chosen or arbitrary shape (Cho et al. 2007). In this study, clump templates were developed to reproduce the irregularly shaped stones used in the experiments as practically as possible. The template may provide a surface description that can be used for the calculation of inertial parameters and visualization of results.

Four distinct stones of those used in the experiments, with sizes ranging between 3.0 and 8.0 cm, were selected from C_1 and C_2 to be created using clump templates as shown in Figs. 5(a and b), respectively. To reproduce realistic stone shapes and sizes, images of individual rocks were taken from various angles using a high-resolution camera. The images were then imported into the commercial 3D computer-aided design (CAD) program, *Rhino 5.0*, to generate the triangular meshes needed for the generation of the clump templates.

The bubble pack algorithm built into *PFC3D* code was used to generate a triangulated clump surface. The template parameters may be adjusted to balance the number of particles in each clump and the smoothness of the surface representation. The effect of these parameters was examined and is presented in Fig. 6. It can be seen that as the overlapping distance, d , between spheres increased, more pebbles were needed to form the shape of the clump resulting in a smoother surface (*PFC3D*). To maintain a balance between the number of pebbles in a clump and the computational cost associated with simulating the entire rock

cluster, the ratio between the largest and smallest particle was kept at 0.3 and the overlap distance was set to 100 as depicted in Fig. 7.

Damping Ratio and Coefficient of Restitution

The impact damping ratio is an important parameter in rockfall collision analysis and is usually used to account for energy dissipation during impact. Of equal importance is the coefficient of restitution (COR), which represents the ratio between the relative velocity postcollision and the relative velocity precollision. The COR is

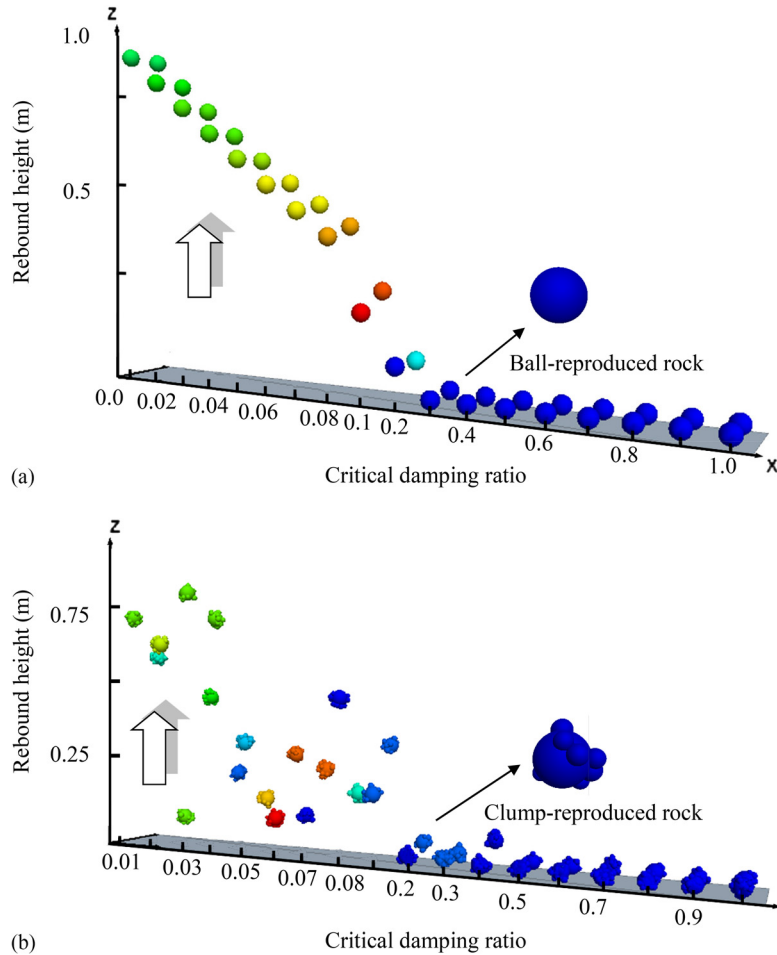


Fig. 8. Discrete element simulation of the drop test: (a) spherical balls; (b) clumps

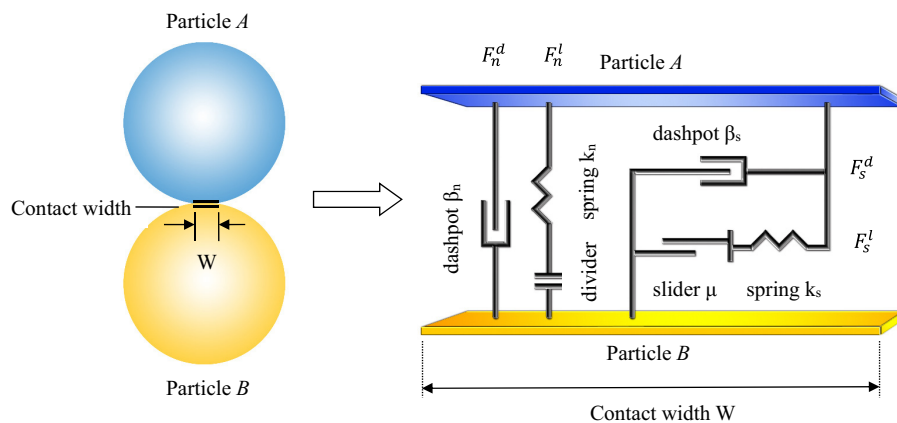


Fig. 9. Rheological components of the linear contact model (adapted from Itasca 2014)

generally regarded as a crucial input parameter that controls the accuracy of rockfall hazard simulation (Chau et al. 2002; Lo et al. 2010; McDowell and Lowndes 2011; Lin and Lin 2015). Therefore, selecting an appropriate COR is important to reproduce a realistic response. In this study, normal and shear dashpots were introduced at each contact to create a viscous damping system as expressed by the following equations:

$$m \frac{d^2x}{dt^2} + c \frac{dx}{dt} + kx = 0 \quad (9)$$

where m = mass; c = damping constant; and k = stiffness.

By defining $\omega = \sqrt{k/m}$ and $d = c/2m$, Eq. (9) can be written in the following form:

$$\frac{d^2x}{dt^2} + 2d \frac{dx}{dt} + \omega^2 x = 0 \quad (10)$$

Substituting a solution of the form $x(t) = Ce^{\lambda t}$ into Eq. (10), the following is written:

$$\lambda^2 + 2d\lambda + \omega^2 = 0 \quad (11)$$

The roots of Eq. (11) can be written as

$$\lambda = -d \pm h \quad (12)$$

where $h = \sqrt{d^2 - \omega^2}$

The solution of Eq. (10) is given by

$$x(t) = C_1 e^{-(d-h)t} + C_2 e^{-(d+h)t} \quad (13)$$

Substituting for d and h of Eq. (13) and rewriting it gives the following:

$$x(t) = C_1 e^{-(\beta - \sqrt{\beta^2 - 1})\omega t} + C_2 e^{-(\beta + \sqrt{\beta^2 - 1})\omega t} \quad (14)$$

where $\beta = c/2\sqrt{km}$, defined as the critical damping ratio.

For underdamped cases, which causes rebounding of two impacting objects, the solution of Eq. (10) is written in the form

$$x(t) = e^{-dt} (D_1 \sin \omega_d t + D_2 \cos \omega_d t) \quad (15)$$

where $\omega_d = \sqrt{\omega^2 - d^2}$

Considering the initial conditions of $x = x_0$, $\dot{x}(t=0) = \dot{x}_0$, and $x_0 = 0$, the following solutions are obtained:

$$x(t) = e^{-\beta \omega t} \left(\frac{\dot{x}_0}{\omega_d} \sin \omega_d t \right) \quad (16)$$

$$\dot{x}(t) = -\beta \omega e^{-\beta \omega t} \left(\frac{\dot{x}_0}{\omega_d} \sin \omega_d t \right) + e^{-\beta \omega t} \dot{x}_0 \cos \omega_d t \quad (17)$$

for which the period and natural frequency of the damped system are $T = 2\pi/\omega_d$ and $f = 1/T = \omega_d/2\pi$, respectively.

At time T (period of oscillation), the system recovers the position at $x = 0$. The velocity of the system is given by

$$\dot{x}(t) = -e^{-\beta \omega (\pi/\omega_d)} \dot{x}_0 \quad (18)$$

The COR can then be expressed in the form

$$\alpha = \frac{\dot{x}(t = \frac{\pi}{\omega_d})}{\dot{x}_0} = e^{-\beta \pi / \sqrt{1 - \beta^2}} \quad (19)$$

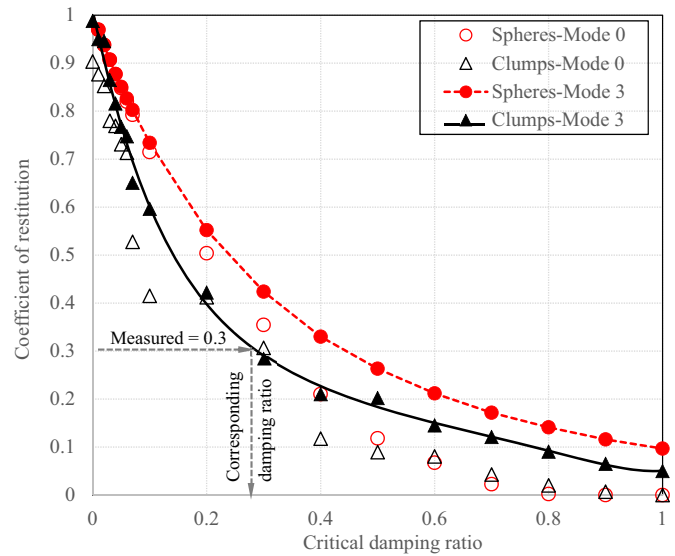


Fig. 10. Relationship between the COR and critical damping ratio for different dashpot modes

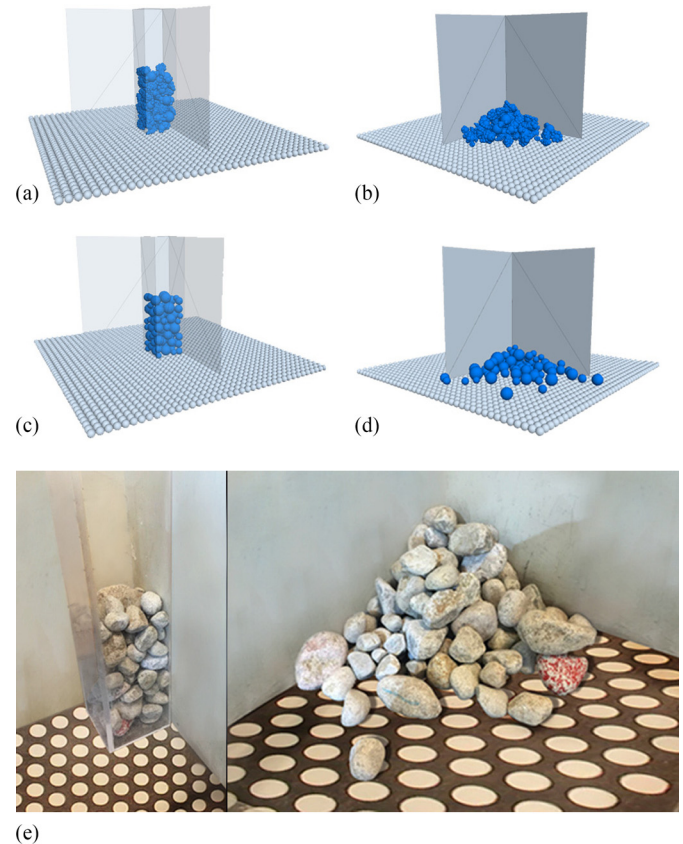


Fig. 11. (a and b) Simulation of the repose angle test using clumps; (c and d) Simulation of the repose angle test using spheres; (e) experimental observations

The COR can be measured in the laboratory using a series of drop tests, and three ratios (Stronge 2000; Ashayer 2007), the kinematic, kinetic, and energy, can be obtained.

The kinematic COR is

$$\alpha = \sqrt{\frac{H_r}{H_i}} \text{ or } \alpha = \frac{V_r}{V_i} \quad (20)$$

where H_r = rebound height; H_i = drop height; and V_r and V_i = magnitude of the postcollision and precollision velocities, respectively.

The kinetic COR is

$$\alpha = \frac{P_t}{P_n} \quad (21)$$

where P_t and P_n = tangential and normal impulse, respectively.

The energy COR is

$$\alpha = \frac{E_r}{E_i} = \frac{\frac{1}{2}mV_r^2}{\frac{1}{2}mV_i^2} = \frac{V_r^2}{V_i^2} \quad (22)$$

where E_i and E_r = translational energies before and after impact; and m = particle mass.

In this study, an average kinematic COR of 0.3 was determined for the rock material in a series of drop tests performed in the laboratory. A summary of the drop test results used to assess the kinematic COR is presented in Table 4. It is noteworthy that the presence of the TactArray sensors may have had an effect on the rebound coefficient. However, because conducting the drop test directly on the sensors might result in significant damage to the

Table 5. Measured Repose Angle of Rocks Using Heap Tests

Test	Angle of repose (degrees)
1	25.9
2	26.2
3	27.0
4	25.5
5	26.6
6	25.7
7	27.1
8	25.3
9	25.2
10	26.5
11	26.8
12	26.5
13	26.6
14	26.4
15	26.0
16	25.9
17	26.1
18	26.0
19	26.1
20	25.8
21	26.7
22	26.7
23	26.2
24	26.4
25	26.0
26	26.2
27	26.3
28	26.6
29	26.4
30	26.2

Note: Average angle of repose = 26.2°; standard deviation = 0.46.

sensing elements, the difference in the measured rebound coefficient using the ebonite sheet and that with the sensing pads was discounted. The tests were then simulated numerically using spherical shaped rocks and clumps of irregular shapes as shown in Figs. 8(a and b). A total of 18 tests were performed by incrementally changing the critical damping ratio from 0 to 1.0 and repeating the analysis using a damping mode, M_d , of either 0 or 3. When M_d is set to 3, no normal-tensile contact force exists between entities; this means that the normal viscous damping force in this mode is capped to ensure that it does not exceed the normal force at the contact.

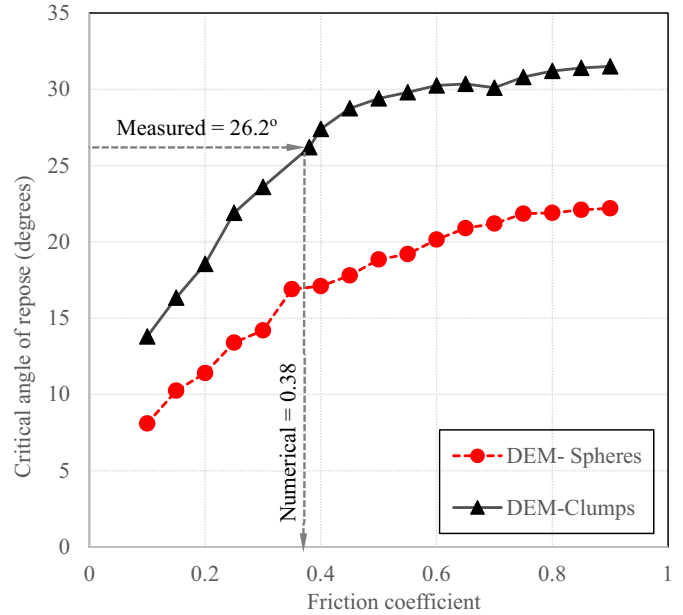


Fig. 12. Relationships between the angle of repose and friction coefficient when particles are modeled using spheres and clumps

Table 6. Input Parameters of the Two Rock Clusters Used in the Experiments

Parameter	Value
Density (kg/m^3)	2,600
Effective modulus	400
Stiffness ratio (k_n/k_s)	1.5
Friction coefficient	0.38
Repose angle (degrees)	26
Normal damping coefficient	0.28

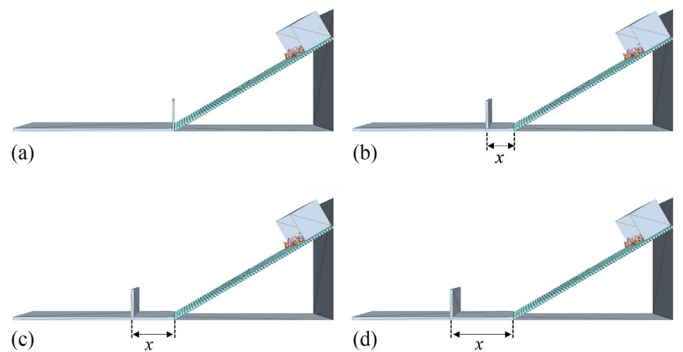


Fig. 13. Discrete element simulation of the flume experiment for different wall distances (in centimeters): (a) $x=0$; (b) $x=25$; (c) $x=40$; (d) $x=60$

This phenomenon can be mathematically expressed as \dot{u}_s = relative shear translational velocity

$$F_n^d = \begin{cases} (2\beta_n \sqrt{m_c k_n}) \dot{u}_n & \text{Dashpot normal force} \\ \min[(2\beta_n \sqrt{m_c k_n}) \dot{u}_n - F_n^l] & \end{cases} \quad (23)$$

$$F_s^d = \begin{cases} (2\beta_s \sqrt{m_c k_s}) \dot{u}_s & \text{Dashpot shear force} \\ 0 & \end{cases} \quad (24)$$

where

$$m_c = \begin{cases} \frac{m^A m^B}{m^A + m^B}, & \text{ball-ball} \\ m^A, & \text{ball-facet} \end{cases};$$

and \dot{u}_s = relative shear translational velocity.

As shown in Fig. 9, the motion of the balls was controlled by a linear spring and dashpot in the normal direction, in which the damping force that opposes the motion was attractive (tension), while the linear-spring force was repulsive (no tension). Depending on the magnitude of the normal velocity, the magnitude of the dashpot force can be larger than that of the spring, and the total normal force, $F_n^l + F_n^d$, is attractive (tension). The no-tension mode prevents this situation from happening by forcing the linear elastic force to be equal to the dashpot force in the normal direction. Furthermore, the shear contact force is in the mode of a slip cut, instead of the full shear, when M_d is 0, where the viscous damping is enforced up to the slip limit, which is controlled by the slider in the shear direction (Fig. 9). As expressed by Eq. (24), if the linear spring is set to slide, then the shear-damping force is zero.

The relationships between the restitution coefficients and damping ratios of both spheres and clumps are presented in Fig. 10. The experimentally measured kinematic COR value was used to determine the corresponding damping ratio according to the model

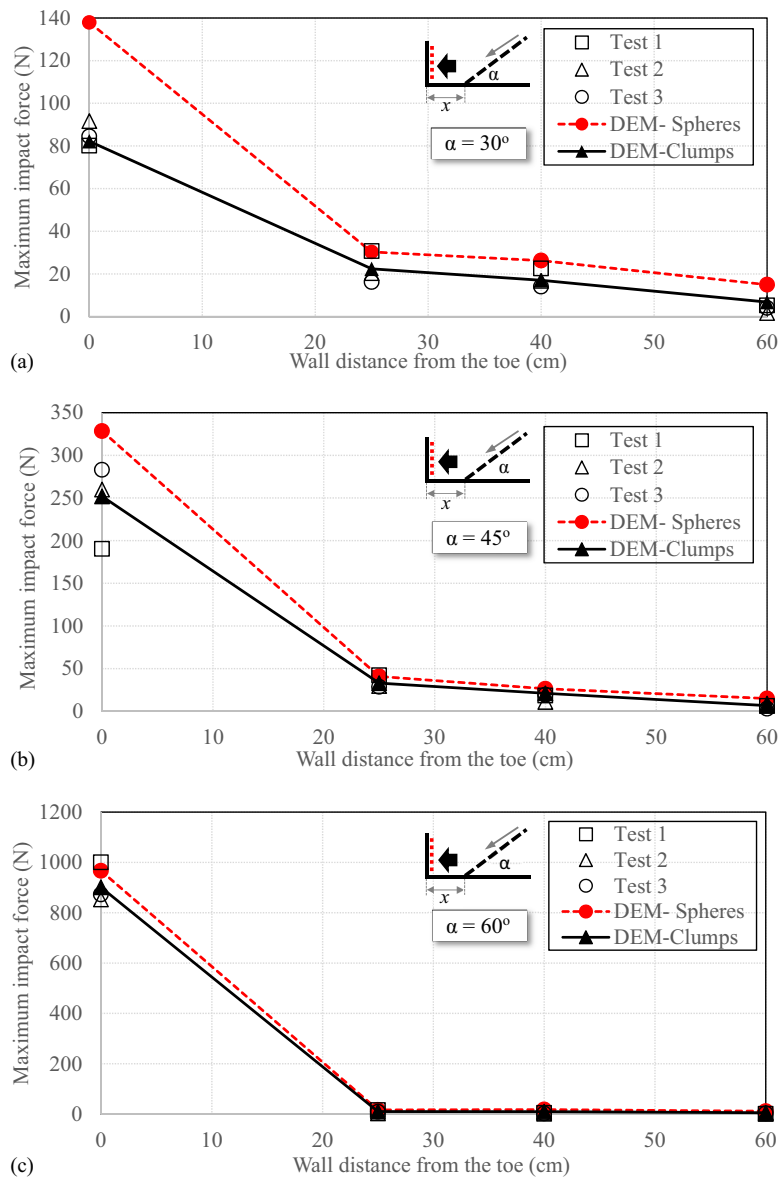


Fig. 14. Calculated and measured impact forces on the wall using rock cluster C_1 for each inclination angle: (a) 30°; (b) 45°; (c) 60°

results for a dashpot mode, M_d , of 3. The critical damping ratio was found to be approximately 0.28.

Coefficient of Friction

Coefficient of friction is another important parameter in modeling the behavior of rockfall using the DEM. It was shown (Zhao 2014; McDowell et al. 2011; Li et al. 2012) that the angle of repose can be used as an approximate estimate of the internal friction angle of the rock cluster. Heap tests were used in this study to measure the angle of repose of the rock material. The width and height of the hopper used in the tests were 0.17 and 0.6 m, respectively. The tests were numerically simulated using the DEM for both spheres and irregularly shaped clumps generated using the clump-template procedure described in the “Modeling the Irregularly Shaped Rock Using Clump Templates” section. As shown in Figs. 11(a and c), the rock cluster was generated within the vertical hopper that was modeled using four walls to form a column. Two adjacent walls were simultaneously deleted allowing the rock cluster to fall under gravity and spread horizontally as depicted in Figs. 11(b and d). A total of 30

laboratory experiments (Table 5) were performed, and the relationships between the angle of repose and the coefficient of friction for particles are shown in Fig. 12. A friction coefficient of 0.38, which corresponded to the measured angle of repose, was determined and used in the rockfall simulation.

Capturing Impact Behaviors

To evaluate the impact of the falling rocks on the barrier wall, a 3D discrete-element model was developed to replicate the laboratory setup. To encourage the development of collision-friction movements, the rough surface was reassembled using layers of spheres arranged in a hexagonal pattern. The diameter of the spheres was chosen such that the slope thickness was equal to that of the horizontal base. A linear-contact model that uses the COR and friction coefficient was used in the analysis. A summary of the micromechanical parameters needed for the discrete element simulation is presented in Table 6. It is noteworthy that the effective contact modulus, E_c , and stiffness ratio, k_t/k_s , used in the analysis were based on those parameters reported by Stahl and Konietzky (2011). The rock

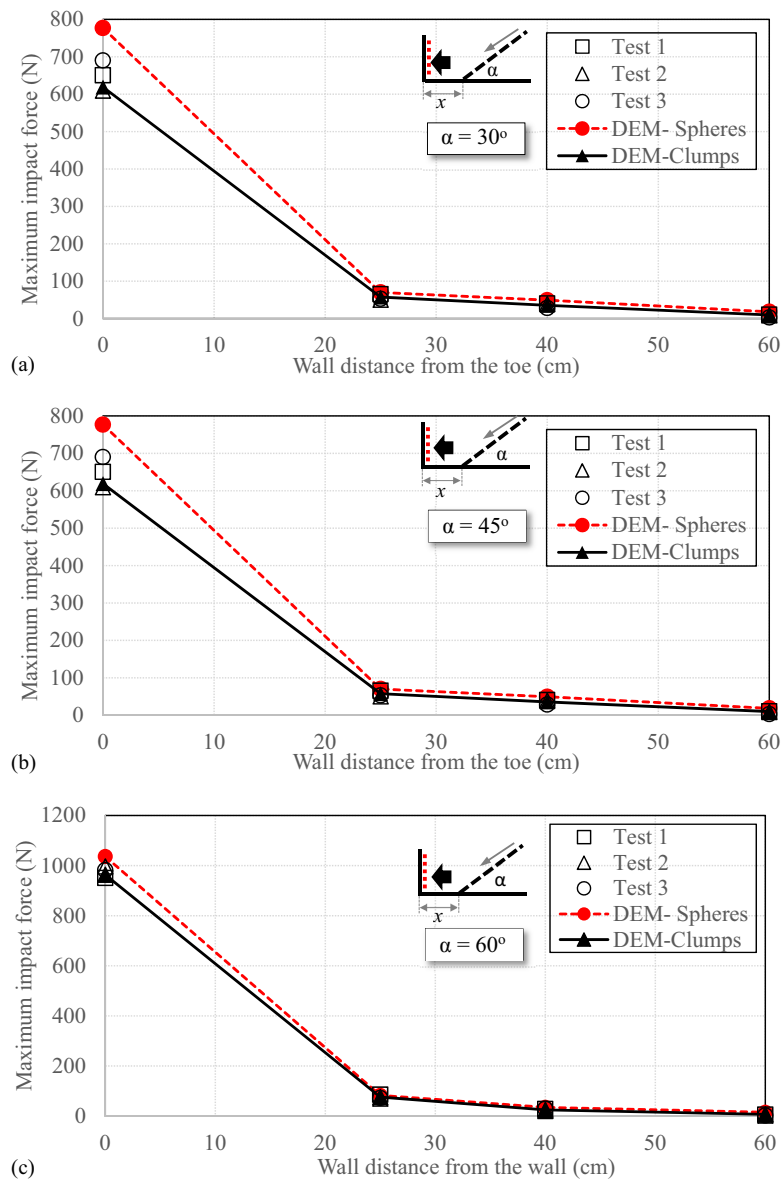


Fig. 15. Measured and calculated impact forces on the wall using rock cluster C_2 for each inclination angle: (a) 30°; (b) 45°; (c) 60°

cluster was randomly generated and allowed to freely move within the release box toward the wall facing the slope. The rock-releasing process was numerically initiated by removing the front wall, which allowed the rocks to move down the slope.

Subroutines were developed in *PFC3D* using the FISH programming language such that the impact information of the two investigated rock clusters was fully recorded (e.g., particle identities, impact times, and impact forces in different directions). Impact forces were chosen to be tracked over impact pressures to facilitate comparison with experimental data. A total of four rockfall simulations were performed for each inclination angle (α of 30, 45, and 60°) considering four different wall distances (x of 0, 25, 40, and 60 cm) from the toe of the slope, as shown in Fig. 13.

Results and Discussions

The impact forces exerted by the two rock clusters on the wall are described in this section. The results obtained from modeling the

stones using spherical particles and the irregularly shaped clumps are then discussed to illustrate the role of rock shape on the impact forces calculated using the discrete-element model. Experimental results (Tests 1, 2, and 3) are used to validate the numerical simulations and a comparison is made between the measured and calculated impact forces. In addition, for cases where the wall was placed at some distance from the toe of the slope, the forces induced by the rock cluster on the horizontal base near the toe of the slope and near the wall were also investigated.

Impact Forces Acting on the Vertical Wall

The changes in impact forces on the vertical wall for different wall locations are presented in Figs. 14 and 15 for rock clusters C_1 and C_2 , respectively. For cluster C_1 , the impact force calculated using irregular rock shapes was found to be approximately 84 N for a slope angle of 30°, which is consistent with the average measured value for x of 0 cm [Fig. 14(a)]. The force rapidly decreased to 25 N (~70%) when the wall offset distance was increased to 25 cm.

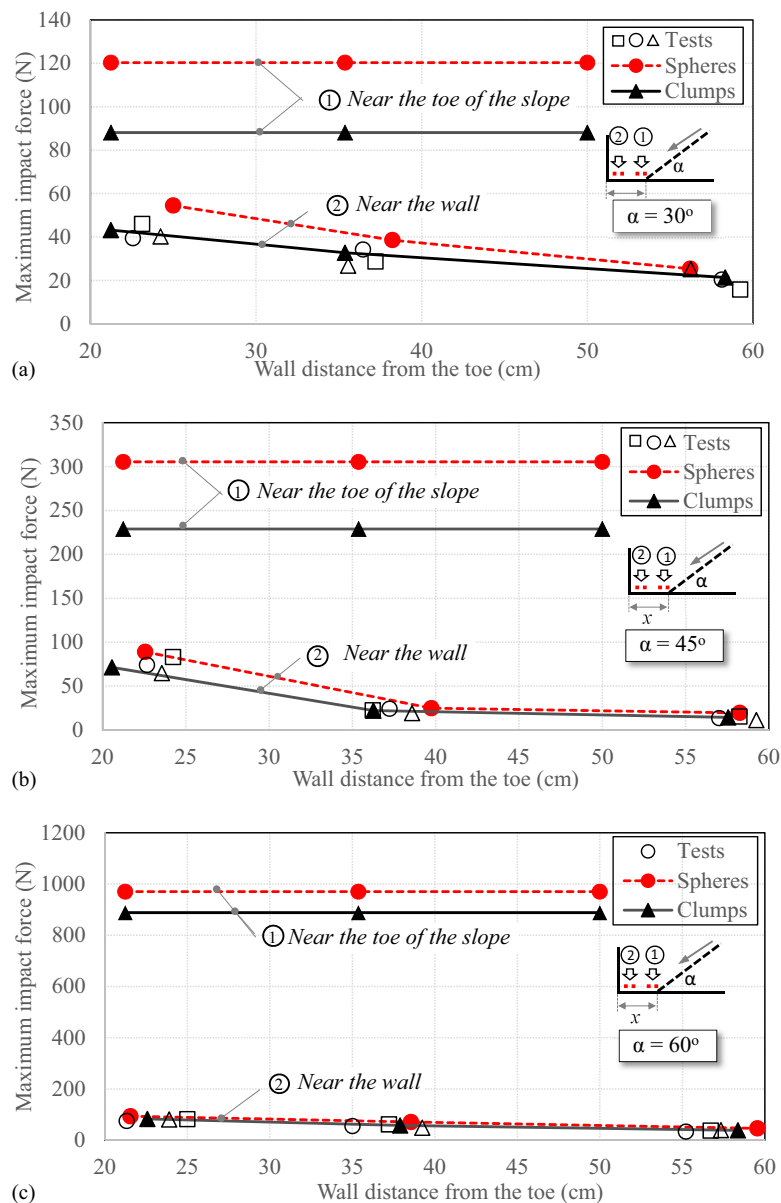


Fig. 16. Measured and calculated impact forces on the base using rock cluster C_1 for each inclination angle: (a) 30°; (b) 45°; (c) 60°

Moving the wall farther from the toe of the slope to distances of 40 and 60 cm resulted in further decreases in forces, to approximately 14 and 4 N, respectively. This finding is attributed to the energy loss due to the rock collision with the horizontal base and along the separation distance before reaching the wall. The impact forces generally increased as the slope angle increased. For an α of 45° , the impact force was found to be approximately 260 N for an x of 0 cm and further increased to 870 N when the slope angle reached 60° . As the wall offset distance increased, the impact forces rapidly decreased to 28 N (89% reduction) and 9 N (99% reduction) for α values of 45 and 60° , respectively. This finding confirms that the steeper the slope, the more energy is lost because of the rock impacting at the base.

Using spherical balls to represent the rock cluster was found to overestimate the impact forces when compared to the measured values, especially for the slope angle of 30° . As shown in Fig. 14(a), an increase in the impact force from 84 to 138 N ($\sim 40\%$) was calculated for x of 0 cm. For slope inclination angles of 45° and 60° , the impact pressures increased at x of 0 cm from 259 and 873 N to 328

and 1,000 N (20 and 13% increases), respectively. For x values of 25, 40, and 60 cm, the difference between the measured and calculated forces for these two slopes was found to be insignificant.

Similar results were found for cluster C_2 , which contained 99 rocks and had a total weight of 13 kg. The impact forces for x of 0 cm were found to be 258, 650, and 976 N for α values of 30° , 45° , and 60° , respectively, as shown in Fig. 15. These values dropped rapidly when the wall was located at some distance from the toe of the slope.

These results suggest that, for the investigated range of parameters, using the clump logic to model falling rocks allows the impact forces to be accurately calculated particularly for slope angles of 30° and 45° . However, approximating the rock shapes using spheres may provide a reasonable estimate of the impact force for a slope angle of 60° ; this may be attributed to the observed sliding mode that dominated the movement of the falling rock cluster over steep slopes. For slope angles of 45° or less, both rolling and bouncing modes governed the particle movement, leading to more a pronounced effect of rock shape on the final impact forces.

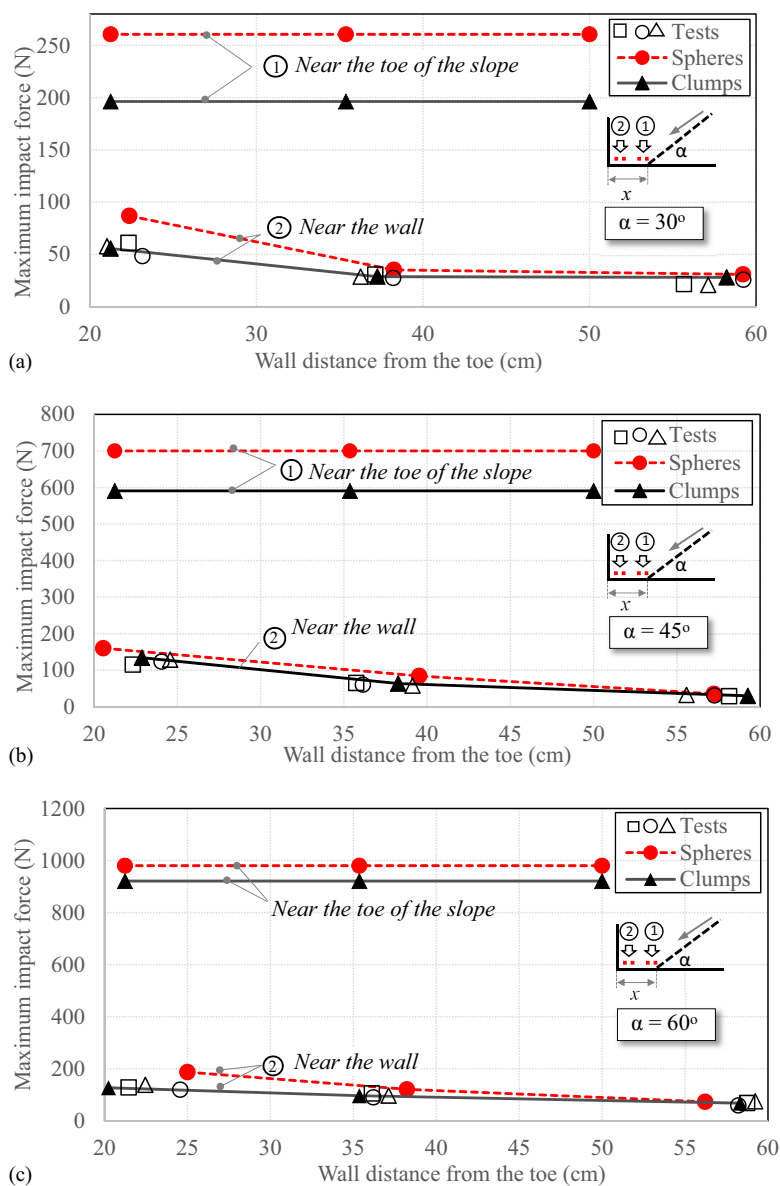


Fig. 17. Calculated and measured impact forces on the flat base using rock cluster C_2 for each inclination angle: (a) 30° ; (b) 45° ; (c) 60°

Impact Forces on the Horizontal Base

The results described in the previous section demonstrated that impact forces are maximum when the wall is located at the toe of the slope. To understand the impact behavior of the falling rock cluster on the landing area if the wall is placed at some distance from the toe of the slope, the numerical model was used to calculate the impact forces on the horizontal base at two different locations: (1) near the toe of the slope and (2) in the area of the vertical wall. The measured forces near the wall (Table 3) were used to validate the numerical results, as shown in Figs. 16 and 17 for clusters C_1 and C_2 , respectively. For rock cluster C_1 , the impact forces near the toe of the 30° slope were calculated to be 88 and 120 N [Fig. 16(a)] when the rocks were modeled using clumps and spheres, respectively. These values increased to 230 and 300 N for clumps and spheres, respectively, at a slope angle of 45° [Fig. 16(b)] and further increased to 888 and 970 N for clumps and spheres, respectively, at a slope angle of 60° [Fig. 16(c)]. Placing the wall away from the toe of the slope resulted in a significant drop in the impact forces because of the energy lost as the particles traveled toward the wall. The changes in the impact forces for different wall locations are shown in Fig. 16 for the three investigated slopes.

Similarly, Fig. 17 shows the impact force at the same locations as those for C_1 along the horizontal base for rock cluster C_2 . The maximum impact forces near the slope, as calculated using irregularly shaped clumps, increased from 200 N for a 30° slope [Fig. 17(a)] to approximately 900 N for a 60° slope [Fig. 17(c)] with a significant drop in value when the wall was placed away from the toe of the slope. Consistent with the results presented in the previous section on vertical walls, using irregularly shaped clumps to simulate the rock cluster resulted in more realistic forces, particularly for the slope angles of 30 and 45°. Both the spheres and clumps produced close results for the slope angle of 60°. It is noteworthy that the maximum impact forces near the toe of the slope (Location 1) were close in magnitude to the forces exerted on the wall at distance x of 0 cm as shown in Figs. 18(a and b) for rock clusters C_1 and C_2 , respectively. This suggests that most of the damage caused by rockfall is likely to happen at the first impacted location.

The effect of the mass of the falling rock cluster can be assessed by comparing the measured impact forces on the wall at x of 0 cm. For the slope inclination angle of 30°, the maximum impact forces caused by cluster C_2 (99 rocks) were found to be approximately 3.5 times the forces caused by C_1 (53 rocks). This effect decreased with an increase in slope angle. No significant difference in impact force was found when the slope angle increased to 60° with maximum impact forces of 1,000 and 920 N for C_1 and C_2 , respectively. This observation signifies that for gentle slopes, the increase in the number of falling rocks results in more interaction among the individual rocks as they roll and bounce down the slope, leading to energy transfer between neighboring rocks in the cluster. For steep slopes, however, because rapid sliding dominates the motion, there is not sufficient time for the rocks to fully disperse, and hence, the interaction effect is minimum.

Summary and Conclusions

The movement of a rock cluster on a rough slope and the impact forces induced on a vertical barrier were investigated using experimental and numerical studies. A physical model was designed and built to allow for the impact forces exerted on a rigid wall to be measured in a controlled environment. Tactile sensing technology was used and square sensing pads were installed on the wall

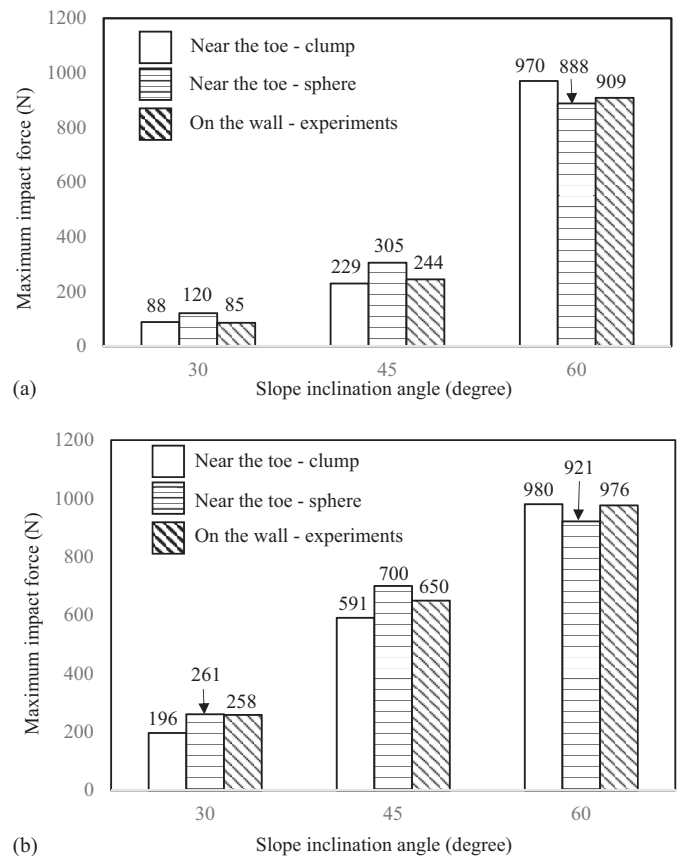


Fig. 18. Comparison of maximum impact forces near the toe of slope and on the wall for rock clusters: (a) C_1 ; (b) C_2

and on the landing surface to record the changes in impact forces for different wall locations and slope inclination angles. Two different rock clusters were used in this study to understand the role of rock volume on the measured results. A 3D discrete-element model was then developed and used to simulate the rough slope and the rock-releasing process. The model was first validated using the experimental data and then used to study the role of rock shape on the impact forces for the investigated range of slope-inclination angles. A series of repose angles and drop tests was performed to determine the friction angle and COR for the rock clusters to use in the numerical analysis. The proposed discrete-element model was proven to be efficient in replicating the rockfall experiments. The modeling results suggest the following:

- Using irregularly shaped clumps to simulate the rock cluster is essential to obtain more realistic impact forces on the wall, particularly for slope angles of 30 and 45°.
- For gentle slopes, the larger the number of simultaneously falling rocks, the more the interaction among the cluster that leads to higher impact forces. For steep slopes, the rocks fall so rapidly, with the sliding mode dominating the motion, that rocks are dispersed and minimum interactions take place among rocks in the falling cluster.
- The presented reduced-scale laboratory experiments and numerical study allowed for the impact forces imposed by falling rock clusters on a rigid wall to be investigated under controlled conditions. Large-scale analysis may be needed to confirm the measured responses for various geometric properties and slope conditions.

Acknowledgments

This research was supported by the Natural Sciences and Engineering Research Council of Canada (NSERC). The financial support provided by the Faculty of Engineering at McGill University to the first author is greatly appreciated.

References

- Agliardi, F., and Crosta, G. B. (2003). "High resolution three-dimensional numerical modelling of rockfalls." *Int. J. Rock Mech. Min. Sci.*, 40(4), 455–471.
- Agliardi, F., Crosta, G. B., and Frattini, P. (2009). "Integrating rockfall risk assessment and countermeasure design by 3D modelling techniques." *Nat. Hazards Earth Syst. Sci.*, 9, 1059–1073.
- Ahmed, M. R., Tran, V. D. H. and Meguid, M. A. (2015). "On the role of geogrid reinforcement in reducing earth pressure on buried pipes: Experimental and numerical investigations." *Soils Found.*, 55(3), 588–599.
- Alejano, L., Pons, B., Bastante, F., Alonso, E., and Stockhausen, H. (2007). "Slope geometry design as a means for controlling rockfalls in quarries." *Int. J. Rock Mech. Min. Sci.*, 44(6), 903–921.
- Ashayer, P. (2007). "Application of rigid body impact mechanics and discrete element modeling to rockfall simulation." Ph.D. thesis, Univ. of Toronto, Toronto.
- Basson, F. R. P. (2012). "Rigid body dynamics for rock fall trajectory simulation." *46th U.S. Rock Mechanics/Geomechanics Symp.*, American Rock Mechanics Association, Richardson, TX.
- Bonilla-Sierra, V., Scholtès, L., Donzé, F. V., and Elmoutie, M. (2015). "Rock slope stability analysis using photogrammetric data and DFN-DEM modelling." *Acta Geotech.*, 10(4), 497–511.
- Chau, K. T., Wong, R. H. C., and Wu, J. J. (2002). "Coefficient of restitution and rotational motions of rockfall impacts." *Int. J. Rock Mech. Min. Sci.*, 39(1), 69–77.
- Chen, G., Zheng, L., Zhang, Y., and Wu, J. (2013). "Numerical simulation in rockfall analysis: A close comparison of 2-D and 3-D DDA." *Rock Mech. Rock Eng.*, 46(3), 527–541.
- Cho, N., Martin, C. D., and Sego, D. C. (2007). "A clumped particle model for rock." *Int. J. Rock Mech. Min. Sci.*, 44(7), 997–1010.
- Cundall, P. A., and Strack, O. D. L. (1979). "A discrete numerical model for granular assemblies." *Géotechnique*, 29(1), 47–65.
- Descouedres, F., and Zimmermann, T. (1987). "Three-dimensional dynamic calculation of rockfalls." *Proc., 6th Int. Congress on Rock Mechanics*, G. Herget and S. Vongpaisal, eds., CRC, Boca Raton, FL, 337–342.
- Frattini, P., Crosta, G., Carrara, A., and Agliardi, F. (2008). "Assessment of rockfall susceptibility by integrating statistical and physically-based approaches." *Geomorphology*, 94, 419–437.
- Giani, G. P., Giacomini, A., Migliazza, M., and Segalini, A. (2004). "Experimental and theoretical studies to improve rock fall analysis and protection work design." *Rock Mech. Rock Eng.*, 37(5), 369–389.
- Guzzetti, F., Crosta, G., Detti, R., and Agliardi, F. (2002). "STONE: A computer program for the three-dimensional simulation of rock-falls." *Comput. Geosci.*, 28(9), 1079–1093.
- Indraratna, B., Ngo, N. T., Rujikiatkamjorn, C., and Vinod, J. S. (2014). "Behavior of fresh and fouled railway ballast subjected to direct shear testing: Discrete element simulation." *Int. J. Geomech.*, 10.1061/(ASCE)GM.1943-5622.0000264, 34–44.
- Itasca Consulting Group. (2014). *Particle flow code in three dimensions (PFC3D)*, Minneapolis.
- Kishi, N., Ikeda, K., Konno, H., and Kawase, R. (2000). "Prototype impact test on rockfall retaining walls and its numerical simulation." *6th Int. Conf., Structures under Shock and Impact VI*, C. A. Brebbia and N. Jones, eds., WIT, Southampton, U.K., 351–360.
- Li, W. C., Li, H. J., Dai, F. C., and Lee, L. M. (2012). "Discrete element modeling of a rainfall-induced flowslide." *Eng. Geol.*, 149, 22–34.
- Lin, C. H., and Lin, M. L. (2015). "Evolution of the large landslide induced by Typhoon Morakot: A case study in the Butangbunasi River, southern Taiwan using the discrete element method." *Eng. Geol.*, 197, 172–187.
- Lo, C. Y., Bolton, M. D., and Cheng, Y. P. (2010). "Velocity fields of granular flows down a rough incline: A DEM investigation." *Granular Matter*, 12(5), 477–482.
- Lu, M., and McDowell, G. R. (2010). "Discrete element modelling of railway ballast under monotonic and cyclic triaxial loading." *Géotechnique*, 60(6), 459–467.
- Magnier, S. A., and Donzé, F. (1998). "Numerical simulations of impacts using a discrete element method." *Mech. Cohesion-Frictional. Mater.*, 3(3), 257–276.
- McDowell, G., Li, H., and Lowndes, I. (2011). "The importance of particle shape in discrete-element modelling particle flow in a chute." *Géotechnique Lett.*, 1(3), 59–64.
- Nicot, F., Cambou, B., and Mazzoleni, G. (2001). "Design of rockfall restraining nets from a discrete element modelling." *Rock Mech. Rock Eng.*, 34(2), 99–118.
- Oda, M., and Iwashita, K. (1999). *Mechanics of granular materials: An introduction*, CRC, Boca Raton, FL.
- PFC3D [Computer software]. Itasca Consulting Group, Minneapolis.
- Plassiard, J.-P., and Donzé, F.-V. (2009). "Rockfall impact parameters on embankments: A discrete element method analysis." *Struct. Eng. Int.*, 19(3), 333–341.
- Rhino 5.0 [Computer software]. Robert McNeel & Associates, Seattle.
- Ritchie, A. M. (1963). "The evaluation of rockfall and its control." *Highway Record No. 17*, Committee on Landslide Investigations, Washington State Highway Commission, Olympia, WA, 13–28.
- Spadari, M., Giacomini, A., Buzzi, O., Fityus, S., and Giani, G. P. (2012). "In situ rockfall testing in New South Wales, Australia." *Int. J. Rock Mech. Min. Sci.*, 49, 84–93.
- Stahl, M., and Konietzky, H. (2011). "Discrete element simulation of ballast and gravel under special consideration of grain-shape, grain-size and relative density." *Granular Matter*, 13(4), 417–428.
- Stronge, W. J. (2000). *Impact mechanics*, Cambridge University Press, Cambridge, U.K.
- Taghavi, R. (2011). "Automatic clump generation based on mid-surface." *2nd International FLAC/DEM Symposium, Continuum and Distinct Element Numerical Modeling in Geomechanics*, Vol. 1, Itasca Consulting Group, Minneapolis, 791–797.
- Thoeni, K., Giacomini, A., Lambert, C., Sloan, S. W., and Carter, J. P. (2014). "A 3D discrete element modelling approach for rockfall analysis with drapery systems." *Int. J. Rock Mech. Min. Sci.*, 68(Jun), 107–119.
- Turner, A. K., and Schuster, R. L. (2013). *Rockfall characterization and control*, Transportation Research Board, National Academy of Sciences, Washington, DC.
- Wang, Y., and Tonon, F. (2011). "Discrete element modeling of rock fragmentation upon impact in rock fall analysis." *Rock Mech. Rock Eng.*, 44(1), 23–35.
- Wei, L.-W., et al. (2014). "The mechanism of rockfall disaster: A case study from Badouzh, Keelung, in northern Taiwan." *Eng. Geol.*, 183, 116–126.
- Zhao, T. (2014). "Investigation of landslide-induced debris flows by the DEM and CFD." Ph.D. thesis, Univ. of Oxford, Oxford, U.K.